IEEE Access
Multidisciplinary | Rapid Review | Open Access Journal

Received January 20, 2020, accepted January 31, 2020, date of publication February 7, 2020, date of current version February 17, 2020.

*Digital Object Identifier 10.1109/ACCESS.2020.2972345*

# Modeling and Adaptive Design of the SRF-PLL: Nonlinear Time-Varying Framework

**BAHRAM SHAKERIGHADI, (Student Member, IEEE), ESMAEIL EBRAHIMZADEH, (Member, IEEE), MADS GRAUNGAARD TAUL, (Senior Member, IEEE), FREDE BLAABJERG, (Fellow, IEEE), AND CLAUS LETH BAK, (Senior Member, IEEE)**

Department of Energy Technology, Aalborg University, 9220 Aalborg, Denmark

Corresponding author: Bahram Shakerighadi (bas@et.aau.dk)

This work was supported by the VILLUM FONDEN under the VILLUM Investigators Grant—Reliable Power Electronic Based Power System (REPEPS).

**ABSTRACT** Synchronous reference frame phase-locked loops (SRF-PLLs) are widely used in different technologies, such as wind turbines, electric vehicles, more electric aircraft, and motor drives, to estimate system's variables. The SRF-PLL is an adaptive notch filter that is used to estimate a sinusoidal signal's amplitude, phase angle, and frequency. However, when the input signal is subjected to a considerable variation or includes a significant noise, its stability and performance become challenging. In this paper, the stability of the SRF-PLL for substantial changes in the input signal's variables are investigated. To do so, the nonlinear time-varying (NTV) model of the system is proposed and is used for the large-signal stability assessment. Then, an adaptive tuning method, based on the proposed NTV model, is designed to improve its transient performance during and after the variation. Simulation and experimental results are used to validate the proposed method.

**INDEX TERMS** Grid-connected voltage source converters, large-signal stability, phase-locked loops, rate-of-change-of-frequency, synchronization.

## I. INTRODUCTION

The voltage magnitude, phase angle, and frequency bring crucial information in control of most power-electronic-based (PE-based) AC devices in different technologies such as wind turbines, more electric aircraft, motor drives, etc., [1]–[5]. Most often, a synchronous reference frame phase-locked loop (SRF-PLL), as a standard PLL, is employed to determine the variables mentioned above [1]. An SRF-PLL is an adaptive notch filter that is used to estimate its input phase [6]. The SRF-PLL is widely used for the synchronization task; however, it is also employed for a wide range of applications such as fault detection, islanding detection, position detection, etc., [7]–[9]. A challenging problem associated with the PLLs is to estimate the system variables in the presence of a large disturbance of the input signal. Focusing on the synchronization performance, it is expected that the SRF-PLL adapts with its input signal fast and is able to reject disturbances [10]. However, this may be challenging when the input signal is noisy by its amplitude, phase angle or frequency [11]. Regarding the noisy input signal, the literature can be divided into three main categories based on:

- Variations in input magnitude: This is mostly related to the voltage dip [1], [12]. As the input signal magnitude affects the SRF-PLL's performance, a large deviation in it may lead the system into an unstable mode [1], [2].
- Variations in input phase angle: Most often, it is related to an unbalanced severe fault in the system or the start-up problem of the PLL [2], [13]–[15].
- Variations in input signal frequency [6]: Different conditions lead to frequency deviation of the system. Either a severe fault or unbalancing between the generations and loads in the electrical system, such as power systems and more electric aircraft, may cause frequency deviation [16], [17].

Researchers often use filters in the input signal (pre-loop filters) or inside of the control loop (in-loop filters) to deal with the polluted input [1]. The concept behind most works regarding the enhancing of performance of synchronization control is to make the PLL less sensitive to its input signal variations [1], [6], [10], [14]. Regarding the magnitude variation of the input, one can use an amplitude normalization

The associate editor coordinating the review of this manuscript and approving it for publication was Guangdeng Zong.

scheme (ANS) in the PLL structure to decouple it by its magnitude [1], [18].

On the other hand, the input phase angle deviation may lead to an unstable situation or an incorrect preventive action. In [13], it is reported that a large amount of grid-connected energy sources are disconnected from the system by the wrong estimation of the frequency using the PLL during a severe fault, viz., the phase jump on the grid side. Incorrect frequency estimation may be critical as the protection systems may be set in a fraction of a second based on the state variables of the system [19]. In [14], an adaptive tuning technique is introduced for the PLL to make the control system robust from its input phase deviation. However, for a large phase jump, the nonlinear model of the PLL is necessary to assess its stability.

A nonlinear model of the PLL brings more accurate information about the system in comparison with the small-signal models [20]–[22]. In [20], a nonlinear model of the grid-tied voltage source converter (VSC) is introduced. The large-signal model of the PLL, in addition to the grid side model, is used to determine the stability margin. However, the impact of the PLL's parameters on large-signal stability is not investigated. In [21], the nonlinear model of the type-1 PLL is presented, and its stability for the phase jump and frequency drift is investigated. Although the SRF-PLL dynamic response to the phase jump and frequency deviation is introduced in [21], its large-signal stability model is not investigated. Moreover, a solution to improve its estimation error during the transient is not discussed. In [23], although the large-signal model of the PLL is introduced, and its stability challenges is presented based on the phase portrait concept, the impact of different input model is not studied. For instance, it is not clear how different frequency deviation models affect the system stability.

Several methods using pre-loop and in-loop filters have been addressed in many works to decrease the frequency deviation impact on the PLL's performance, [24]–[26]. In all the latter references, the performance of the PLL concerning the frequency variation is improved. However, only the small-signal model of the control system is discussed for both the stability assessment and the performance. Therefore, the effectiveness of the proposed methods is not investigated under severe system frequency deviations. In [6], the PLL is modeled as a nonlinear time-invariant system, and the phase portrait diagram is used to assess the system stability. In [6], it is mentioned that the PLL is a nonlinear time-varying (NTV) system, in which parameters change by time; however, the SRF-PLL stability for various frequency deviation scenarios is not investigated. The major challenge is to design the PLL that is able to deal with the large signal deviation of the system characteristics.

This paper aims to assess the impact of the input signal deviation on the large-signal stability model of the SRF-PLL. Based on the large-signal stability assessment, an adaptive model of the SRF-PLL is introduced that is able to overcome frequency estimation errors caused by the noisy input signals. In this way, the NTV model of the SRF-PLL is presented. After that, different phase jump and frequency deviation models are implemented as the input of the system. Mathematically, it is proved that as long as the energy function constraints of the system are satisfied, the system can follow the input's frequency and stand stable. Based on the proposed model for the large-signal stability, an SRF-PLL with an adaptive loop gain is designed that is capable of keeping its stability during frequency deviation and phase jump, while its bandwidth is not affected. Considering the NTV model of the SRF-PLL and the proposed adaptive model to enhance its stability during a large disturbance, the main contributions of this paper are:

- Introducing the NTV model of the SRF-PLL based on the voltage dips, phase jump, and the frequency deviation. This NTV model includes nonlinear terms of the system, which are of the interest of large-signal stability assessment.
- Large-signal stability assessment of the SRF-PLL based on its NTV model. The proposed model depicts the dynamic of the system during the transient. Therefore, it is recommended to use it as a tool for tuning the system parameters during a large disturbance in the system.
- Proposing an adaptive solution that increases the stability margin of the SRF-PLL during a large disturbance of the frequency and phase angle in the system. The proposed method changes the SRF-PLL parameters during the transition. However, neither the order of the system increases nor the parameters are changed for the steady state condition.

The rest of the paper is organized as follows. Section II defines different concepts regarding the frequency deviation and the phase jump in the system. The NTV model of the SRF-PLL regarding the phase jump and frequency deviations are proposed in Section III. Section IV discuss the stability for different case studies of the phase jump and frequency deviations through the simulation results. Section V presents an adaptive design for the SRF-PLL to overcome stability challenges. Conclusions are presented in Section VI.

## II. DISTURBANCE IN POWER SYSTEMS

PE-based electrical systems are dynamic in their nature, which means that their state variables change continuously. Three important variables that indicate the system stability conditions are voltage magnitude, phase angle, and its frequency. In this section, the concept behind these three categories of the system, namely voltage magnitude variations, phase jump, and the frequency drift, are discussed. An illustrative example tested on the IEEE 39-bus test system is used in order to show the various concepts.

### A. VOLTAGE DEVIATION OF THE SYSTEM

Voltage deviation in the system may happen either gradually or within a short period. Basically, increasing the system load leads to a decrease in the voltage magnitude; however, this

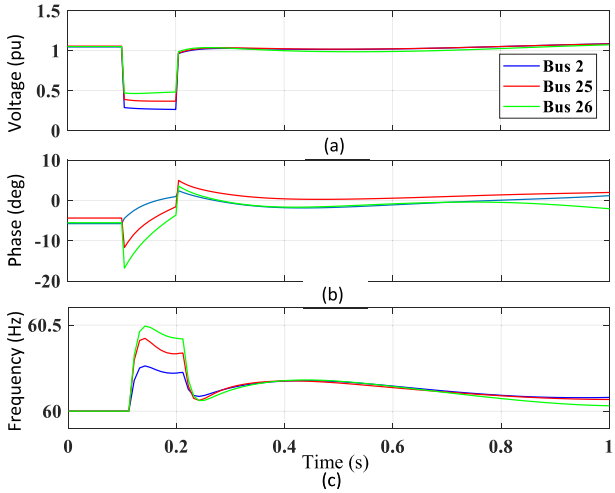


**FIGURE 1.** (a) Voltage magnitude, (b) phase angle, and (c) frequency of Bus 2, 25, and 26 of the IEEE 39-bus test system subjected to a three-phase short circuit at t = 0.1 s and cleared at t = 0.2 s.

happens slowly. On the other hand, a severe fault, such as a three-phase short circuit in the transmission line, causes a voltage dip or a voltage sag. For instance, a three-phase short circuit event on the line 2-3 of the IEEE-39-bus test system causes voltage dip in the buses close to the event location. The fault starts at t = 100 ms and is cleared after 100 ms. Fig. 1(a) shows the voltage magnitudes of Bus 2, 25, and 26, which are close to the line 2-3. The fault causes a voltage dip instantaneously after the fault. Bus 2 is closer to the line 2-3; therefore, its voltage magnitude is subjected to a larger deviation in comparison with other buses.

### B. PHASE JUMP

The phase jump, also known as the phase shift, may happen in the system either unintentionally due to a fault, black start, etc. [13], [14], or deliberately for the sake of power transferring facilitation [27]. Most often, voltage drops are associated with phase jumps [28]. Fig. 1(b) shows the change in the phase angle of Bus 2, 25, and 26. The phase jump can be detected after the fault instantaneously. The phase jump can cause critical challenges for various system components, especially PE-based units controlled in direct-quadrature (dq) frame, because the phase angle is used for changing the control frame [5].

### C. FREQUENCY DEVIATION

The frequency, as a global state of the system, is known as one of the most important key points in evaluation of the system condition, and may change for different reasons in various electrical applications. For instance, a line trip may cause frequency deviations as shown in Fig. 1(c). In PE-based power systems, the frequency may change because of unbalance between loads and generations. Most often, the frequency deviation in power systems should be in a specific range ( a fraction of a Hertz), so the system works in its normal condition [19]. However, the frequency should be determined appropriately for a system subjected to a severe fault, in which the frequency drift may exceed some Hertz from the fundamental value. In more electric aircraft, frequency changes between 350 and 800 Hz, in order to adjust the engine speed with a desired value [16]. With this in mind, determining the frequency deviation is important in PE-based electric systems.

The frequency deviation is mostly defined as its rate of change, called rate-of-change-of-frequency (ROCOF), which is determined as follows:

$$ROCOF = \frac{df}{dt} \tag{1}$$

where $f$ and $t$ are the frequency and time, respectively. Practically, ROCOF is calculated based on the average of the frequency deviation over a measuring window, given as follows [29]:

$$ROCOF \triangleq \frac{1}{N_r}\sum_{i=1}^{N_r}\left(\frac{\Delta f_i}{\Delta t_r}\right) \tag{2}$$

where $N_r$ is the sampling number and $\Delta f_i$ is the $i_t h$ frequency change during $\Delta t_r$ period. However, a linear equivalent model, shown as follows, can be used as the ROCOF equivalent:

$$f = f_0 + Rt \tag{3}$$

where $f_0$ and $R$ are the steady-state frequency and the ROCOF value, respectively. However, the frequency change can be a function of time with a higher order. For instance, in [13], the frequency change is presented as a second order deviation during a severe fault in the system. In fact, the true modeling of the ROCOF can significantly affect the frequency estimation, especially when a PLL is used to determine the frequency of the system.

## III. NONLINEAR TIME-VARYING MODEL OF THE SRF-PLL

Accurate modeling of the PLL is needed to evaluate the stability margin and tune its parameter. The block diagram of a SRF-PLL is shown in Fig. 2(a), while its small-signal model is illustrated in Fig. 2(b). This model has been investigated extensively in the literature [1]. Although the small-signal model of the PLL gives an adequate approximation of the system behavior as long as the system is in a quasi-locked state, it cannot accurately predict the actual behavior of the real system subjected to a large disturbance. Therefore, a nonlinear model of the PLL, as shown in Fig. 2(c), provides a higher accuracy. The discrepancy between the small-signal and large-signal model of the PLL shows an outstanding division during large disturbances. The aim of the SRF-PLL is to estimate the three-phase grid voltage signal's parameters, which is given as follows:

$$\upsilon(t) = V_{pcc}\cos\overbrace{(\omega t + \varphi)}^{\theta} \tag{4}$$

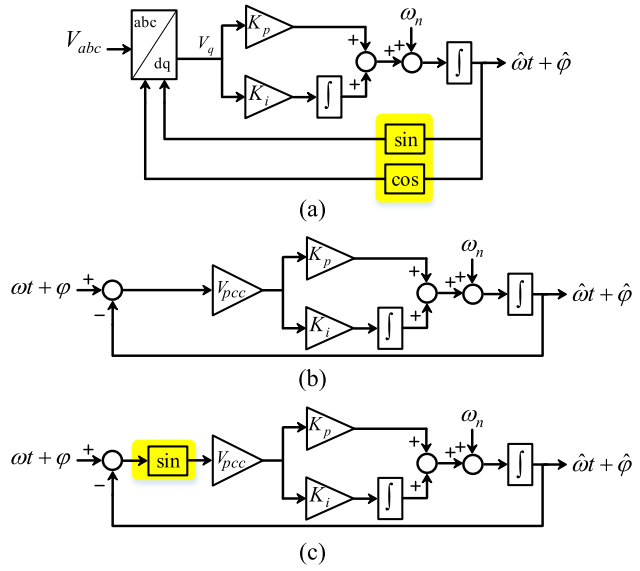


**FIGURE 2.** SRF-PLL analysis (a) Block diagram of the SRF-PLL. (b) Its linear model. (c) Its nonlinear model.

where $V_{pcc}$, $\theta$, $\varphi$, and $\omega$ are the input signal amplitude, phase angle, initial phase angle, and angular frequency of the point of common coupling (PCC), respectively. The output of the SRF-PLL can be used for the estimation of the input signal's parameters, given as follows:

$$\hat{v}(t) = \hat{V}_{pcc} \cos\overbrace{\left(\hat{\omega}t + \hat{\varphi}\right)}^{\hat{\theta}} \tag{5}$$

where $\hat{V}_{pcc}$, $\hat{\theta}$, $\hat{\varphi}$, and $\hat{\omega}$ are the estimated values of input signal amplitude, phase angle, initial phase angle, and angular frequency, respectively. It is worth mentioning that system variables are time dependent, due to the integrator in the PI controller. Although the time dependency is eliminated in small-signal model of the PLL, it is applied to the large-signal model. This is shown later in (10).

In this paper, as the frequency changes gradually, a phase jump is defined as the step change in $\varphi$, while frequency deviation relates to the change in $\omega$. Therefore, phase jumps and frequency deviations are analyzed separately. However, frequency deviation leads to phase change.

### A. THE SRF-PLL DYNAMIC RESPONSE CONSIDERING VOLTAGE MAGNITUDE CHANGE

Considering Fig. 2(c), the control loop gain is related to the PCC's voltage magnitude. The following equation shows the estimated phase angle to its input:

$$\hat{\theta} = \int \left[ V_{pcc} K_p \sin\left(\theta - \hat{\theta}\right) + K_i \int V_{pcc} \sin\left(\theta - \hat{\theta}\right) dt + \omega_n \right] dt \tag{6}$$

where $\hat{\theta}$ and $\theta$ are the estimated and actual voltage phase angle, respectively. $\omega_n$ is the nominal frequency value in rad/sec, which is typically equal to $100\pi$ or $120\pi$. $K_p$ and $K_i$ are the proportional and integral gains of the PLL. $V_{pcc}$ indicates the voltage magnitude of the PCC. A simple method to make the control system insensitive from the PCC voltage magnitude, is to use the normalized value of the $V_q$, as shown in Fig. 3. This technique has been well established in the literature [1]. Therefore, sensitivity analysis to the voltage magnitude can be eliminated from the large-signal stability assessment of the SRF-PLL.

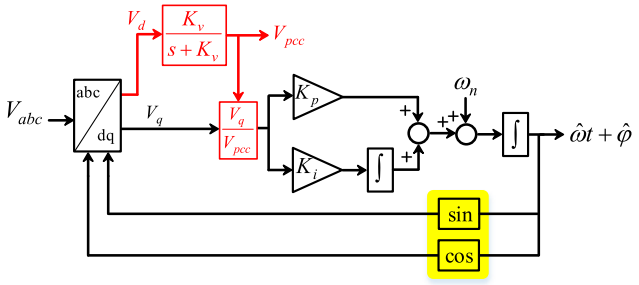


**FIGURE 3.** The SRF-PLL using normalized magnitude (in red).

### B. LARGE-SIGNAL MODEL OF THE SRF-PLL CONSIDERING THE PHASE ANGLE DEVIATION

In order to evaluate the stability of the PLL subjected to a large deviation in the phase angle of the input, a linear approximation is not valid anymore. Therefore, in order to evaluate the phase jump impact on the nonlinear model of the SRF-PLL, one can assume (6) with a fix input frequency and magnitude. Therefore, $\ddot{\theta} = 0$ and $\dot{V}_{pcc} = 0$. By using two times derivative of both sides of the equation, the following equation can be obtained:

$$\ddot{\hat{\theta}} = \left(\dot{\theta} - \dot{\hat{\theta}}\right) V_{pcc} K_p \cos\left(\theta - \hat{\theta}\right) + V_{pcc} K_i \sin\left(\theta - \hat{\theta}\right). \tag{7}$$

Now, by defining $x_1 = \left(\theta - \hat{\theta}\right)$ and $x_2 = \left(\dot{\theta} - \dot{\hat{\theta}}\right)$, the following model can be represented:

$$\begin{cases} \dot{x}_1 = x_2 \\ \dot{x}_2 = -\left[V_{pcc} K_p x_2 \cos(x_1) + V_{pcc} K_i \sin(x_1)\right]. \end{cases} \tag{8}$$

As parameters are fixed by time, (8) presents a nonlinear time-invariant state-space model of the SRF-PLL. The frequency deviation is studied in the next part.

### C. LARGE-SIGNAL MODEL OF THE SRF-PLL CONSIDERING THE FREQUENCY DEVIATION

Considering the nonlinear model of the SRF-PLL, shown in Fig. 2(c), one can show its mathematical model given as follows:

$$\hat{\omega} = \omega_n + \left(K_p + K_i \int\right)\left[V_{pcc} \sin\left(\omega t - \hat{\omega} t\right)\right] \tag{9}$$

where $\hat{\omega}$ is the estimated frequency in rad/s, and $K_p$ and $K_i$ are the SRF-PLL's proportional and integral gain, respectively. The initial phase angle of the input signal is considered as a

fixed value, and the focus of the study is only on the frequency deviation of the system.

Using the first order deviation with respect to the time of (9) and rewrite it, the following nonlinear time-varying model of the estimated frequency is obtained as:

$$\dot{\hat{\omega}} = \dot{\omega} + \left[ \frac{V_{pcc}K_p\left(\omega - \hat{\omega}\right)\cos\left(\omega t - \hat{\omega}t\right)}{1 + V_{pcc}K_p t\cos\left(\omega t - \hat{\omega}t\right)} + \frac{V_{PCC}K_i\sin\left(\omega t - \hat{\omega}t\right) - \dot{\omega}}{1 + V_{pcc}K_p t\cos\left(\omega t - \hat{\omega}t\right)} - \frac{\dot{\omega}}{1 + V_{pcc}K_p t\cos\left(\omega t - \hat{\omega}t\right)} \right]. \quad (10)$$

The model is time-varying as $t$ appears in the denominator of the right side of (10), and it is nonlinear due to the sin and cos operator in (10). For the initial point at $t = t_0$, the estimated ROCOF is obtained as $\dot{\hat{\omega}}_{t_0} = V_{PCC}K_p\left(\omega_{t_0} - \hat{\omega}_{t_0}\right)$, which also can be concluded from Fig. 2(b). In addition, the final value of the estimated ROCOF in a stable case in an infinite time is $\dot{\omega}$, which means that if the SRF-PLL works in its stable mode, it will follow the frequency change. However tracing the frequency change is a challenge that needs to be clarified using the stability assessment, as the operating point is a time variant variable, which is discussed in the next section.

## IV. STABILITY ASSESSMENT OF THE PROPOSED MODEL FOR THE SRF-PLL

### A. LARGE-SIGNAL STABILITY ASSESSMENT OF THE SRF-PLL CONSIDERING THE PHASE JUMP

In order to evaluate the stability status of the model, the vector fields of the state variables can be used. Regarding the concept of the vector fields, by mapping $\dot{x}_1$ and $\dot{x}_2$ on the $(x_1 - x_2)$ plane, for every initial value of $(x_{10} - x_{20})$, the subsequent value of the $(x_1 - x_2)$ can be computed. The vector fields of the PLL nonlinear model are shown in Fig. 4. The arrows in Fig. 4 show that for every initial value of the state variables, the system state will follow a trajectory, also called state trajectories.

It is worth to mention that the initial value of the state variables plays a critical role in determining the state trajectories. In order to determine the initial value for the phase error $(x_1)$ and its velocity $(x_2)$, consider that the system works in its steady state condition. In this condition, the phase error is equal to zero. A phase jump $(\Delta\theta)$ in the input signal of the PLL makes the initial value of the phase error equal to the phase jump. The reason is that the estimated phase cannot change instantly. The initial value for the frequency error can be estimated as follows:

$$\left(\dot{\theta} - \dot{\hat{\theta}}\right)_{init.} = -K_P V\sin\left(\theta - \hat{\theta}\right)_{init.} \quad (11)$$

where the subscript *init*. denotes initial values. The integrator is eliminated in the initial value calculations as integrators have a gradual response to a step change. The state trajectories of the SRF-PLL with $K_p = 0.2$ and $K_i = 2$ are shown in Fig. 4, which are typical values. In the next section, it will be discussed how the phase jump in the PLL input may cause a transient instability.

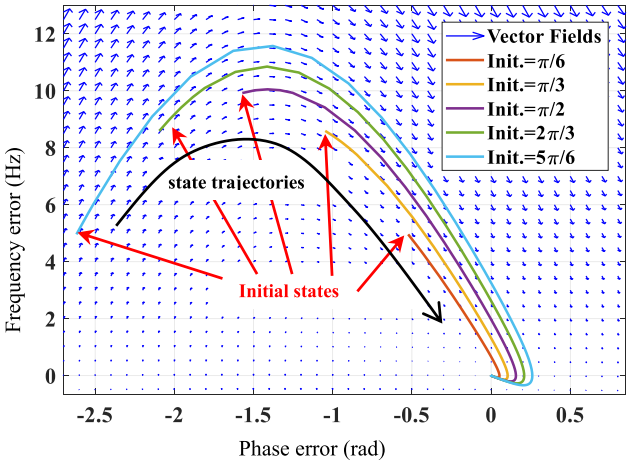


**FIGURE 4.** State trajectory of the nonlinear model of the PLL for different initial values (Init.) of the phase jump.

Apparently, the SRF-PLL stands stable considering any initial condition of the phase jump in its input signal. However, considering the frequency error caused by the phase jump may lead to a frequency protection trip. In conventional systems, the frequency is allowed to vary based on the supply and load imbalance. There is a limitation for the frequency variation based on the international standards [20], [30]. Therefore, if an undesired frequency variation is detected in the system, then the protection system should act. Regarding the transient frequency change in the system based on the mentioned standard [30], if a frequency less than 56.4 Hz or greater than 61.7 Hz for a nominal value of 60 Hz is detected, then the protection system should act instantaneously. As an important example, detecting the under-frequency by the PLL is reported as one of the main reasons for the energy interruption in California in [13], which leads to 1.2 GVA loss of generation.

### B. LARGE-SIGNAL STABILITY ASSESSMENT OF THE SRF-PLL CONSIDERING THE FREQUENCY DEVIATION

In order to evaluate the SRF-PLL stability, the estimated frequency should converge to the input frequency at infinity. Therefore, based on (10), the second term on the right side should converge to zero at infinity. This can be shown as follows:

$$\lim_{t\to\infty}\left[ \frac{V_{PCC}K_p\left(\omega - \hat{\omega}\right)\cos\left(\omega t - \hat{\omega}t\right)}{1 + V_{PCC}K_p t\cos\left(\omega t - \hat{\omega}t\right)} + \frac{V_{PCC}K_i\sin\left(\omega t - \hat{\omega}t\right) - \dot{\omega}}{1 + V_{PCC}K_p t\cos\left(\omega t - \hat{\omega}t\right)} - \frac{\dot{\omega}}{1 + V_{PCC}K_p t\cos\left(\omega t - \hat{\omega}t\right)} \right] = 0. \quad (12)$$

As $\omega$ and $\hat{\omega}$ vary with respect to the time, only the first term in the numinator and the second term in the denominator are considered for a large value of t. Therefore, (12) can be simplified as follows:

$$\lim_{t\to\infty} \frac{\omega - \hat{\omega}}{t} = 0. \tag{13}$$

Simply, for the first order equivalent of the system frequency, the order of the nominator in (9) is equal to its denominator's order. However, for orders higher that one of the nominator of (9), the system stability needs more evaluation. This is investigated by using the energy function and is shown through case studies, as discussed in the following.

Regarding the large-signal stability of the SRF-PLL's NTV model in (10), one can define the Lyapunov function to determine the stability margins. In this way, the following energy function based on the system frequency error is defined as:

$$V = \frac{1}{2}P\left(\hat{\omega} - \omega\right)^2 \tag{14}$$

where P is a positive real value. In order to work in stable condition, the Lyapunov function and its derivative with respect to the time should be positive and negative, respectively. From (14), it can be concluded that the Lyapunov function is always positive; however, its derivative with respect to the time is introduced as (15), shown at the bottom of this page, which has a significant impact on determining the stability margins. Eq. (15) can be rewritten as (16), shown at the bottom of this page.

Assuming $-\pi/2 \le \left(\omega - \hat{\omega}\right)t \le \pi/2$ (which is a reasonable assumption), the first two terms on the right side of (16) are always negative. On the other hand, as $\hat{\omega}$ follows $\omega$ with a lag, then by increasing $\omega$, $\dot{\omega}$ is positive, while $\left(\hat{\omega} - \omega\right)$ is negative. This is also true for the decreasing of $\omega$. Therefore, the third term on the right side of (16) is positive. With this in mind, In order to have a negative value for (15), which leads to global stability of the system, the following inequality should be valid:

For positive values of $\dot{\omega}$ :

$$V_{pcc}K_p\left(\omega - \hat{\omega}\right)\cos\left(\omega t - \hat{\omega}t\right) + V_{pcc}K_i\sin\left(\omega t - \hat{\omega}t\right) \ge \dot{\omega}$$

For negative values of $\dot{\omega}$ :

$$V_{pcc}K_p\left(\omega - \hat{\omega}\right)\cos\left(\omega t - \hat{\omega}t\right) + V_{pcc}K_i\sin\left(\omega t - \hat{\omega}t\right) \le \dot{\omega}. \tag{17}$$

However, for both negative and positive values of $\dot{\omega}$, the following inequality can be concluded by using some linearization techniques:

$$\frac{\dot{\omega} - V_{PCC}K_p\left(\omega - \hat{\omega}\right)}{V_{PCC}K_i\left(\omega - \hat{\omega}\right)} \le t. \tag{18}$$

Eq. (18) can be rewritten as follows:

$$|\dot{\omega}| \le K_p\left|V_{PCC}\left(\omega - \hat{\omega}\right)\right| + K_i t\left|V_{PCC}\left(\omega - \hat{\omega}\right)\right|. \tag{19}$$

For a conservative case, if $t \ll \epsilon$, in which $t \ll \epsilon$ is a small positive value, the following inequality should be valid in order to have a stable condition:

$$|\dot{\omega}| \le K_p V_{PCC}\left|\omega - \hat{\omega}\right|. \tag{20}$$

The conservative case means that the system change happens instantaneously.

It can be concluded from (19) and (20) that despite of the order of input deviation, if the proportional and integral gains are tuned appropriately so the Lyapunov inequalities are satisfied, then the system works in its stable condition. This means that if the damping term of the error is larger than the frequency change, then the system will stand stable. However, if the frequency changes faster than it could be damped, then the estimated frequency error will become larger and larger. Although this is a general conclusion, which can also be derived by the small-signal models, one can use the Lyapunov inequalities for tuning the SRF-PLL's parameters in order to guarantee the system stability.

## V. DESIGN AND PERFORMANCE ANALYSIS

In this section, the SRF-PLL's response for different types of variations in the input signal is presented. In the first part, the SRF-PLL's response to the phase jump is illustrated. After that, its response to the first and second order frequency deviations are show. Then, an adaptive design of the SRF-PLL for damping the frequency impact on the system stability is proposed.

### A. SRF-PLL'S RESPONSE TO THE PHASE JUMP IN THE INPUT SIGNAL

In order to evaluate the large-signal stability of the PLL, different phase jumps are considered in the input signal. Fig. 5 shows the state trajectories of the system for different phase jumps between $-\pi$ to $\pi$. For phase jumps more than $\pi/2$ or less than $-\pi/2$, the frequency error will increase and then decrease until it reaches the origin point. The stable and unstable regions for the frequency stability are determined based on the standards [30], shown Fig. 5.

$$\dot{V} = \left[P\left(\hat{\omega} - \omega\right)\right] \times \left[\frac{V_{pcc}K_p\left(\omega - \hat{\omega}\right)\cos\left(\omega t - \hat{\omega}t\right) + V_{pcc}K_i\sin\left(\omega t - \hat{\omega}t\right) - \dot{\omega}}{1 + V_{pcc}K_p t\cos\left(\omega t - \hat{\omega}t\right)}\right]. \tag{15}$$

$$\dot{V} = \underbrace{\frac{-PV_{pcc}K_p\left(\hat{\omega} - \omega\right)^2\cos\left(\left(\omega - \hat{\omega}\right)t\right)}{1 + V_{pcc}K_p t\cos\left(\omega t - \hat{\omega}t\right)}}_{-} + \underbrace{\frac{PV_{pcc}K_i\left(\hat{\omega} - \omega\right)\sin\left(\left(\omega - \hat{\omega}\right)t\right)}{1 + V_{pcc}K_p t\cos\left(\omega t - \hat{\omega}t\right)}}_{-} + \underbrace{\frac{-P\dot{\omega}\left(\hat{\omega} - \omega\right)}{1 + V_{pcc}K_p t\cos\left(\omega t - \hat{\omega}t\right)}}_{+}. \tag{16}$$

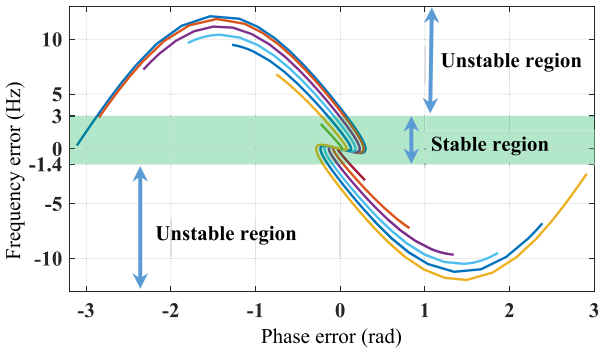


**FIGURE 5.** Transient stability analysis of the SRF-PLL based on proposed state trajectories.

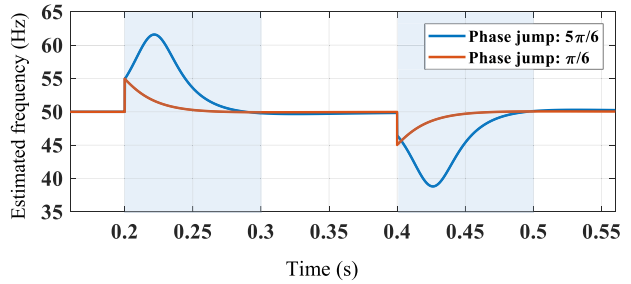


**FIGURE 6.** Time domain simulations of the SRF-PLL subjected to different phase jumps.

Hence, if the transient frequency limit is violated, then it is expected that the system works on its unstable transient mode, and the protection systems may act subsequently. This may lead to undesired trip of the converter and loss of generation [13].

A time domain simulation including $\pi/6$ and $5\pi/6$ phase jumps at t = 0.2 s, and $-\pi/6$ and $-5\pi/6$ phase jumps at t = 0.4 s for the SRF-PLL is illustrated in Fig. 6. It can be seen that the proposed large-signal model shows exactly the same result with the nonlinear time-domain simulations, which is for each initial value of the phase jump, the trend and the maximum value of the estimated frequency is exactly the same.

In order to verify the proposed method and the simulations, experimental tests are done for the SRF-PLL with the same configuration, shown in Fig. 7. The PLL is modeled as an open loop control system. To emulate the PLL input, the grid simulator manufactured by Chroma is used, and the PLL system is implemented in dSPACE DS1007 system. The dSPACE can be programmed using the block diagram environment in MATLAB/Simulink. The SRF-PLL estimated frequency error for different phase jumps are shown in Fig. 8. Although the frequency of the input is constant, the estimated frequency of the SRF-PLL presents a transient error, which may lead to a protection system action [13]. In order to avoid an undesired protection trip, it is recommended to consider a large-signal stability model of the SRF-PLL in the design of it.

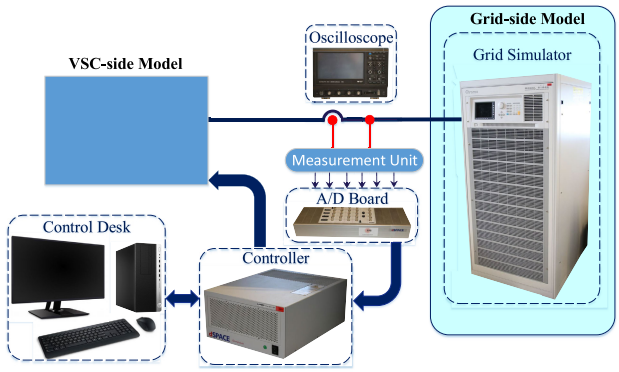


**FIGURE 7.** (a) Experimental setup at Aalborg University. (b) Laboratory setup used to evaluate the estimated frequency of the SRF-PLL.

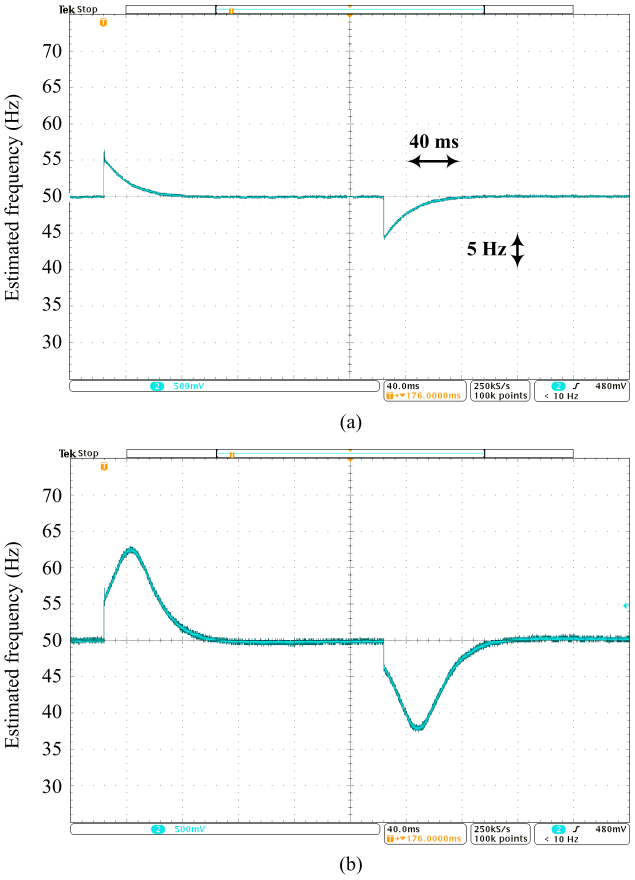


**FIGURE 8.** The SRF-PLL estimated frequency for different phase-jumps (experimental results). (a)$\pi/6$, and (b) $5\pi/6$ phase jump implement to the PLL and are cleared after 200 ms.

It is worth mentioning that the PLL is a feedback control loop, which is used in the VSC control system. Therefore, its performance can be affected by VSC DC voltage and the main grid dynamic, in addition to other control loops with the same dynamic time constant. In this way, the PLL may cause system instability, for instance for the weak grid, which is out of the scope of this paper [2].

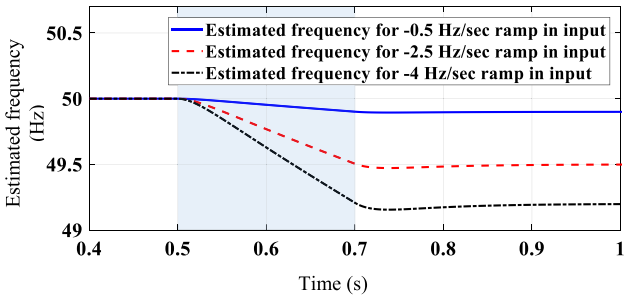


**FIGURE 9.** Estimated frequency by the SRF-PLL for different first order frequency deviation at the input signal.

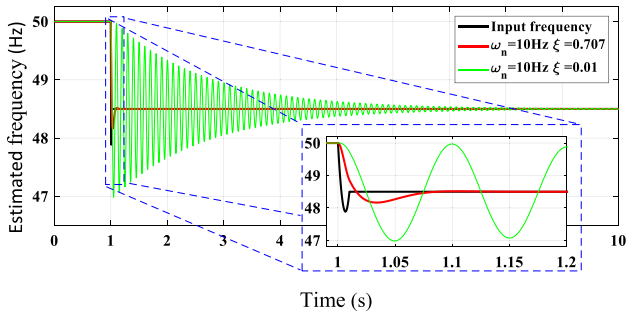


**FIGURE 10.** Estimated frequency by the SRF-PLL with standard dapmping and very small damping coefficients considering a second order frequency deviations at the input signal.

### B. SRF-PLL'S RESPONSE TO THE FREQUENCY DEVIATIONS OF THE INPUT SIGNAL

In this part, only the first and second order deviations of the frequency are investigated. Fig. 9. shows the simulation result of the estimated frequency considering the first order frequency deviations in the input with different rate of change. As it can be seen in Fig. 9, for instance, for a 2.5 Hz/sec frequency deduction over a 0.2-second period, the estimated frequency decreases from 50 Hz to 49.5 Hz, which means that the frequency estimator follows the input frequency with the first order deviation. To exaggerate the results of the PLL's performance, two case studies of the simulation results are mentioned in Fig. 10 with a normal and a very low damping factors. For a frequency deviation from 50 Hz to 48.5 Hz during 10 ms period from t = 1 s to t = 1.01 s with a quadratic polynomial function, the estimated frequency might not follow the input frequency. Although the system is stable (even for a low damping factor, shown in Fig. 10), the transient behavior of the system is not appropriate for a low damping factor. Therefore, the system needs consideration with respect to its parameter tuning, which is discussed in the next part.

### C. DESIGN: ADAPTIVE TUNING OF THE SRF-PLL

A conservative solution to overcome stability problem is to modify system parameters during the frequency deviation. To do so, considering (20), if the input frequency changes with the velocity of $\dot{\omega}$, then the system should be able to damp it with a rate of $K_p V_{PCC} \left|\omega - \hat{\omega}\right|$, which should be more than system change in order to keep the system stable. In this way,

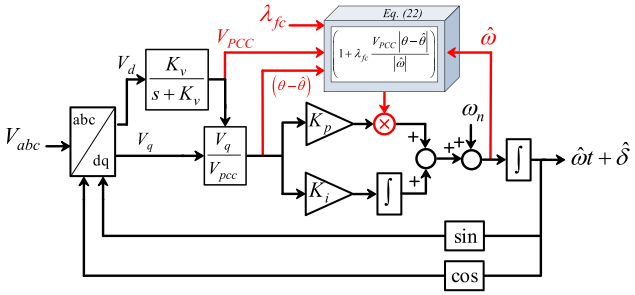


**FIGURE 11.** Block diagram of the proposed adaptive SRF-PLL.

one can increase the damping factor, $K_p$, during the transient. In this way, $K_p$ should have an appropriate value during the transient. Considering (20), by using an integration from both side of the inequality, following inequality can be obtained:

$$1 \leq \frac{K_p V_{pcc} \left|\theta - \hat{\theta}\right|}{|\omega|}. \tag{21}$$

Therefore, $K_p$ is designed in an adaptive manner in order to change during the frequency deviation so (15) is satisfied. If $K_p$ modified as follows, the system will stand stable during the frequency change.

$$K_p \rightarrow K_p \left(1 + \lambda_{fc} \frac{V_{PCC} \left|\theta - \hat{\theta}\right|}{\left|\hat{\omega}\right|}\right) \tag{22}$$

where instead of $\omega$ in (21), one can use its estimated value and assume that the system will stand stable during the frequency deviation. $\lambda_{fc}$, called damping factor, is the a positive constant value that set in a manner to keep (15) satisfied. The simulation result of the adaptive SRF-PLL is shown in Fig. 11. In order to make the design more general, so the system performance improve for all system changes, a normalized form of the PLL is used. Therefore, the modified PLL is insensitive to the voltage magnitude change of the input signal.

To exaggerate the results, consider a system with a bandwidth of 10 Hz and a very low damping factor of 0.01, ($\omega_n = 10\,Hz$, $\xi = 0.01$). Obviously, such a low damping factor will not be intentionally set in the control where an often used approach is to design for a damping ratio of 0.707. However, as described in [2], [31], [32], the overall effective damping associated with the synchronization loop may be lower than this value during weak-grid and grid-fault conditions. Accordingly, this low damping ratio is used here as a test case for such severe conditions where the effective damping ratio of the system may reach very low or negative values. As the simulation result shown in Fig. 12, the PLL exhibits weakly damping oscillations under a frequency deviation from 50 Hz to 48.5 Hz for a period of 10 ms. However, if the proposed adaptive method is used in order to damp the transient deviation of the system, then the system stands stable and shows an appropriate performance. The estimated frequency of the SRF-PLL using different damping factors is illustrated in Fig. 12. As the damping factor $(\lambda_{fc})$ increases,

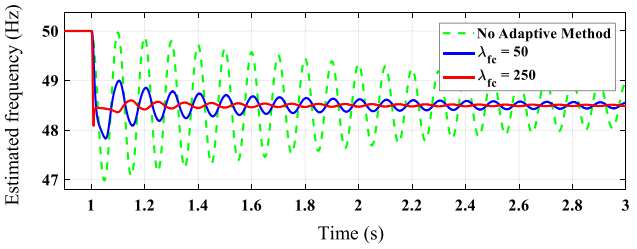


**FIGURE 12.** Estimated frequency by the SRF-PLL for second order input frequency deviation from t = 1 s to t = 1.01 s using the proposed adaptive tuning method with different damping factors.

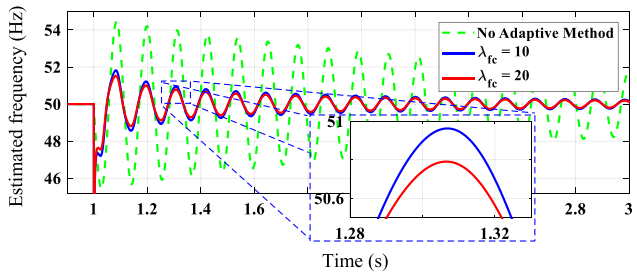


**FIGURE 13.** Estimated frequency by the SRF-PLL for 30° phase jump at t = 1 s using the proposed adaptive tuning method with different damping factors.

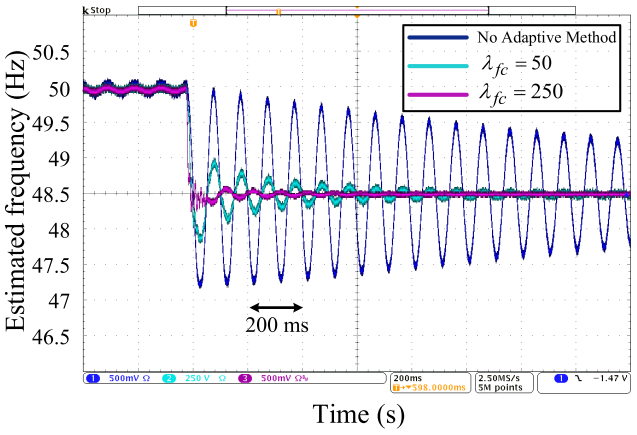


**FIGURE 14.** Experimental results of the estimated frequency by the SRF-PLL for second order input frequency deviation using the proposed adaptive tuning method with different damping factors.

the input deviation will be damped on the output signal. However, the oscillation after change may not be damped, as the parameters are only adapted during the change, and they will come back to its initial values after the change. It is also worth mentioning that the system parameters are only adapted during the transition of the frequency; while it has a fixed value during the normal condition of the system. In other words, based on (22), the adaptive method is only changing the SRF-PLL's parameter in case that the input variables are changing.

On the other hand, by increasing the system damping during the change, it is expected to have a better performance for phase jump. The proposed design is tested for the phase jump scenario, and the simulation results are shown

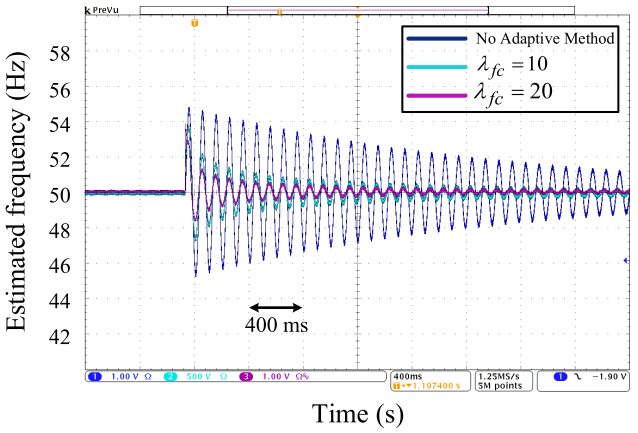


**FIGURE 15.** Experimental results of the estimated frequency by the SRF-PLL for 30° phase jump using the proposed adaptive tuning method with different damping factors.

in Fig. 13. In this scenario, system parameters are set as for the frequency deviation scenario with different damping factors. It is shown in Fig. 13 that the system performance is improved as the damping factor increases. In order to have the best performance for both phase jump and frequency deviation, an appropriate value of the $(\lambda_{fc})$ should be chosen, which can be selected based on the required performance.

To demonstrate the effectiveness of the proposed method, some simulation results are presented in Fig. 14 and Fig. 15. These experimental results are obtained by using the configuration shown in Fig. 7. In this way, Simulation results of the frequency deviation and phase jump case studies shown in Fig. 12 and Fig. 13, are verified with the experimental setup and presented in Fig. 14 and Fig. 15, respectively.

## VI. CONCLUSION

In this paper, a nonlinear time-varying model of the SRF-PLL is introduced in order to evaluate its performance for different types of input frequency deviations and phase jumps. To do so, first, the NTV model of the SRF-PLL is presented. Based on the NTV model, the system stability is assessed for large disturbances. In this way, nonlinear stability assessment techniques, such as the Lyapunov stability and the phase portrait are used to determine stability margins. Thereafter, based on the proposed model and its stability assessment, an adaptive method is proposed for the SRF-PLL design, so the system performance is improved for different input frequency deviations and phase jumps. The proposed model and the performance of the designed SRF-PLL are verified by using simulation and experimental results. By using the proposed adaptive model of the SRF-PLL, improved results are accomplished when the system is subjected to a large disturbance in its input phase angle and frequency.

## REFERENCES

[1] S. Golestan, J. M. Guerrero, and J. C. Vasquez, "Three-phase PLLs: A review of recent advances," *IEEE Trans. Power Electron.*, vol. 32, no. 3, pp. 1894–1907, Mar. 2017.

[2] M. G. Taul, X. Wang, P. Davari, and F. Blaabjerg, "An overview of assessment methods for synchronization stability of grid-connected converters under severe symmetrical grid faults," *IEEE Trans. Power Electron.*, vol. 34, no. 10, pp. 9655–9670, Oct. 2019.
[3] S. Bifaretti, P. Zanchetta, and E. Lavopa, "Comparison of two three-phase PLL systems for more electric aircraft converters," *IEEE Trans. Power Electron.*, vol. 29, no. 12, pp. 6810–6820, Dec. 2014.
[4] R. T. Ryan, D. N. Hogan, R. J. Morrison, and J. G. Hayes, "Digital closed-loop control strategy to maintain the phase shift of a multi-channel BCM boost converter for PFC applications," *IEEE Trans. Power Electron.*, vol. 34, no. 7, pp. 7001–7012, Jul. 2019.
[5] F. Blaabjerg, R. Teodorescu, M. Liserre, and A. Timbus, "Overview of control and grid synchronization for distributed power generation systems," *IEEE Trans. Ind. Electron.*, vol. 53, no. 5, pp. 1398–1409, Oct. 2006.
[6] M. Karimi-Ghartemani and A. K. Ziarani, "Performance characterization of a non-linear system as both an adaptive notch filter and a phase-locked loop," *Int. J. Adapt. Control Signal Process.*, vol. 18, no. 1, pp. 23–53, Feb. 2004.
[7] M. Ciobotaru, V. G. Agelidis, R. Teodorescu, and F. Blaabjerg, "Accurate and less-disturbing active antiislanding method based on PLL for grid-connected converters," *IEEE Trans. Power Electron.*, vol. 25, no. 6, pp. 1576–1584, Jun. 2010.
[8] X. Song, B. Han, S. Zheng, and S. Chen, "A novel sensorless rotor position detection method for high-speed surface pm motors in a wide speed range," *IEEE Trans. Power Electron.*, vol. 33, no. 8, pp. 7083–7093, Aug. 2018.
[9] D. Dong, B. Wen, P. Mattavelli, D. Boroyevich, and Y. Xue, "Modeling and design of islanding detection using phase-locked loops in three-phase grid-interface power converters," *IEEE J. Emerg. Sel. Topics Power Electron.*, vol. 2, no. 4, pp. 1032–1040, Dec. 2014.
[10] S. Golestan, J. M. Guerrero, and J. C. Vasquez, "A robust and fast synchronization technique for adverse grid conditions," *IEEE Trans. Ind. Electron.*, vol. 64, no. 4, pp. 3188–3194, Apr. 2017.
[11] L. Wang, Q. Jiang, L. Hong, C. Zhang, and Y. Wei, "A novel phase-locked loop based on frequency detector and initial phase angle detector," *IEEE Trans. Power Electron.*, vol. 28, no. 10, pp. 4538–4549, Oct. 2013.
[12] H. A. Hamed, A. F. Abdou, E. H. E. Bayoumi, and E. E. EL-Kholy, "A fast recovery technique for grid-connected converters after short dips using a hybrid structure PLL," *IEEE Trans. Ind. Electron.*, vol. 65, no. 4, pp. 3056–3068, Apr. 2018.
[13] NERC/WECC Inverter Task Force, "1200 MW fault induced solar photovoltaic resource interruption disturbance report: Southern California 8/16/2016 event," NERC, Atlanta, GA, USA, Tech. Rep., Jun. 2017.
[14] M. K. Ghartemani, S. A. Khajehoddin, P. K. Jain, and A. Bakhshai, "Problems of startup and phase jumps in PLL systems," *IEEE Trans. Power Electron.*, vol. 27, no. 4, pp. 1830–1838, Apr. 2012.
[15] C. Liu, X. Tian, K. Chen, Y. Su, and Y. Li, "Effect of PLL on transient performance of wind turbines generator under voltage phase jump," *J. Eng.*, vol. 2019, no. 16, pp. 967–971, Mar. 2019.
[16] B. Sarlioglu and C. T. Morris, "More electric aircraft: Review, challenges, and opportunities for commercial transport aircraft," *IEEE Trans. Transp. Electrific.*, vol. 1, no. 1, pp. 54–64, Jun. 2015.
[17] H. Bevrani, *Robust Power System Frequency Control*. Cham, Switzerland: Springer, 2014.
[18] J. Hu, Q. Hu, B. Wang, H. Tang, and Y. Chi, "Small signal instability of PLL-synchronized type-4 wind turbines connected to high-impedance AC grid during LVRT," *IEEE Trans. Energy Convers.*, vol. 31, no. 4, pp. 1676–1687, Dec. 2016.
[19] *IEEE Standard for Interconnection and Interoperability of Distributed Energy Resources With Associated Electric Power Systems Interfaces*, Standard IEEE 1547-2018 (Revision IEEE Std 1547-2003), Apr. 2018, pp. 1–138.
[20] K. Lentijo and D. F. Opila, "Minimizing inverter self-synchronization due to reactive power injection on weak grids," in *Proc. IEEE Energy Convers. Congr. Exposit. (ECCE)*, Sep. 2015, pp. 1136–1142.
[21] S. Golestan, F. D. Freijedo, A. Vidal, J. M. Guerrero, and J. Doval-Gandoy, "A quasi-type-1 phase-locked loop structure," *IEEE Trans. Power Electron.*, vol. 29, no. 12, pp. 6264–6270, Dec. 2014.
[22] J. Zhao, M. Huang, and X. Zha, "Transient stability analysis of grid-connected VSIs via PLL interaction," in *Proc. IEEE Int. Power Electron. Appl. Conf. Exposit. (PEAC)*, Nov. 2018, pp. 1–6.
[23] H. Wu and X. Wang, "Transient stability impact of the phase-locked loop on grid-connected voltage source converters," in *Proc. Int. Power Electron. Conf. (IPEC-Niigata-ECCE Asia)*, May 2018, pp. 2673–2680.
[24] S. Golestan, F. D. Freijedo, A. Vidal, A. G. Yepes, J. M. Guerrero, and J. Doval-Gandoy, "An efficient implementation of generalized delayed signal cancellation PLL," *IEEE Trans. Power Electron.*, vol. 31, no. 2, pp. 1085–1094, Feb. 2016.
[25] F. A. S. Neves, M. C. Cavalcanti, H. E. P. De Souza, E. J. Bueno, and M. Rizo, "A generalized delayed signal cancellation method for detecting fundamental-frequency positive-sequence three-phase signals," *IEEE Trans. Power Del.*, vol. 25, no. 3, pp. 1816–1825, Jul. 2010.
[26] S. Golestan, E. Ebrahimzadeh, J. M. Guerrero, J. C. Vasquez, and F. Blaabjerg, "An adaptive least-error squares filter-based phase-locked loop for synchronization and signal decomposition purposes," *IEEE Trans. Ind. Electron.*, vol. 64, no. 1, pp. 336–346, Jan. 2017.
[27] B. Hobbs, G. Drayton, E. Bartholomew Fisher, and W. Lise, "Improved transmission representations in oligopolistic market models: Quadratic losses, phase shifters, and DC lines," *IEEE Trans. Power Syst.*, vol. 23, no. 3, pp. 1018–1029, Aug. 2008.
[28] G. S. Kumar, B. K. Kumar, and M. K. Mishra, "Mitigation of voltage sags with phase jumps by UPQC with PSO-based ANFIS," *IEEE Trans. Power Del.*, vol. 26, no. 4, pp. 2761–2773, Oct. 2011.
[29] T. Amraee, M. G. Darebaghi, A. Soroudi, and A. Keane, "Probabilistic under frequency load shedding considering RoCoF relays of distributed generators," *IEEE Trans. Power Syst.*, vol. 33, no. 4, pp. 3587–3598, Jul. 2018.
[30] *IEEE Guide for Abnormal Frequency Protection for Power Generating Plants*, Standard IEEE C37.106-2003 (Revision of ANSI/IEEE Std C37.106-1987), 2004, pp. 1–41.
[31] H. Wu and X. Wang, "Design-oriented transient stability analysis of grid-connected converters with power synchronization control," *IEEE Trans. Ind. Electron.*, vol. 66, no. 8, pp. 6473–6482, Aug. 2019.
[32] M. G. Taul, X. Wang, P. Davari, and F. Blaabjerg, "Systematic approach for transient stability evaluation of grid-tied converters during power system faults," in *Proc. IEEE Energy Convers. Congr. Exposit. (ECCE)*, Sep. 2019, pp. 5191–5198.

**BAHRAM SHAKERIGHADI** (Student Member, IEEE) received the B.Sc. degree from the University of Mazandaran, Iran, in 2010, and the M.Sc. degree from the University of Tehran, Iran, in 2014. He is currently pursuing the Ph.D. degree in modeling and stability assessment of the power electronic-based power systems with the Department of Energy Technology, Aalborg University, Denmark.

He is also a Visiting Researcher with ABB Corporate Research, Västerås, Sweden. His current research interests include modeling and stability assessment of power electronic-based power systems, and control of gird-tied voltage source converters.

**ESMAEIL EBRAHIMZADEH** (Member, IEEE) received the M.Sc. degree in electrical engineering from University of Tehran, Tehran, Iran, in 2012. In 2015, he was employed as a Ph.D. Fellow with the Department of Energy Technology, Aalborg University, Aalborg, Denmark. He has been a Consultant Research and Development Engineer at Vestas Wind Systems A/S, Aarhus, Denmark, in 2017, where he is currently working as a Lead Engineer. His research interests include modeling, design, and control of power-electronic converters in different applications, and power quality and stability analysis in large wind power plants. He received the Best Paper Awards at IEEE PEDG 2016 and IEEE PES GM 2017.

**MADS GRAUNGAARD TAUL** (Senior Member, IEEE) received the B.Sc. and M.Sc. degrees in energy technology with specializing in electrical energy engineering and power electronics and drives from Aalborg University, Denmark, in 2016 and 2019, respectively. He is currently pursuing the Ph.D. degree in power electronic systems with the Department of Energy Technology, Aalborg University, Denmark. His main research interests include renewable energy sources and grid-connected converters with a special focus on modeling and control of power electronics-based power systems under grid fault conditions. In connection with the M.Sc. degree, in 2019, he received the first prize master's thesis award for excellent and innovative project work by the Energy Sponsor Programme.

**FREDE BLAABJERG** (Fellow, IEEE) received the Ph.D. degree in electrical engineering from Aalborg University, in 1995. He was with ABB-Scandia, Randers, Denmark, from 1987 to 1988. He became an Assistant Professor, in 1992; an Associate Professor, in 1996; and a Full Professor of power electronics and drives, in 1998. In 2017, he became a Villum Investigator. He has published more than 600 journal articles in the fields of power electronics and its applications. He has coauthored of four monographs and editor of ten books in power electronics and its applications. His current research interests include power electronics and its applications such as in wind turbines, PV systems, reliability, harmonics, and adjustable speed drives.

He has received 31 IEEE Prize Paper Awards, the IEEE PELS Distinguished Service Award, in 2009, the EPE-PEMC Council Award, in 2010, the IEEE William E. Newell Power Electronics Award 2014, the Villum Kann Rasmussen Research Award 2014, and the Global Energy Prize in 2019. He received the honoris causa at University Politehnica Timisoara (UPT), Romania, and Tallinn Technical University (TTU), Estonia. He was the Editor-in-Chief of the IEEE TRANSACTIONS ON POWER ELECTRONICS, from 2006 to 2012. He has been a Distinguished Lecturer for the IEEE Power Electronics Society, from 2005 to 2007, and for the IEEE Industry Applications Society, from 2010 to 2011 and 2017 to 2018. Since 2019, he has been the President of the IEEE Power Electronics Society. He is also the Vice President of the Danish Academy of Technical Sciences. He was nominated by Thomson Reuters as one of the most 250 cited researchers in engineering in the world, from 2014–2018.

**CLAUS LETH BAK** (Senior Member, IEEE) was born in Århus, Denmark, in April 1965. He received the B.Sc. degree (Hons.) in electrical power engineering and the M.Sc. degree in electrical power engineering from the Department of Energy Technology, Aalborg University, in 1992 and 1994, respectively, and received the Ph.D. degree with the thesis EHV/HV underground cables in the transmission system, in 2015. After his studies, he worked as a Professional Engineer with electric power transmission and substations with specializations within the area of power system protection at the NV Net Transmission System Operator. In 1999, he was employed as an Assistant Professor at the Department of Energy Technology, Aalborg University, where he is currently a Full Professor. He serves as Head of the Energy Technology Ph.D. Program (+ 130 PhD's) and as the Head of the Section of Electric Power Systems and High Voltage and is a member of the Ph.D. board at the Faculty of Engineering and Science. He has supervised/co-supervised more than 35 Ph.D. and 50 M.Sc. theses. His main research areas include corona phenomena on overhead lines, composite transmission towers, power system modeling and transient simulations, underground cable transmission, power system harmonics, power system protection, composite materials for EHV power pylons, and HVDC-VSC offshore transmission networks. He has authored or coauthored approximately 340 publications. He is a member of Cigré SC C4 AG1 and SC B5. He has received the DPSP 2014 Best Paper Award and the PEDG 2016 Best Paper Award. He was the Chairman of the Danish Cigré National Committee, in August 2018.